ACS APPLIED MATERIALS & INTERFACES

Research Article

www.acsami.org

Chlorotoxin-Conjugated Multifunctional Dendrimers Labeled with Radionuclide ^{131}I for Single Photon Emission Computed Tomography Imaging and Radiotherapy of Gliomas

Lingzhou Zhao,[†,⊥] Jingyi Zhu,[‡,⊥] Yongjun Cheng,[†] Zhijuan Xiong,[§] Yueqin Tang,[∥] Lilei Guo,[†] Xiangyang Shi,[*,‡,§] and Jinhua Zhao[*,†]

[†]Department of Nuclear Medicine, Shanghai General Hospital, School of Medicine, Shanghai Jiaotong University, Shanghai 200080, People's Republic of China

[‡]State Key Laboratory for Modification of Chemical Fibers and Polymer Materials, College of Materials Science and Engineering, Donghua University, Shanghai 201620, People's Republic of China

[§]College of Chemistry, Chemical Engineering and Biotechnology, Donghua University, Shanghai 201620, People's Republic of China

[∥]Experiment Center, Shanghai General Hospital, School of Medicine, Shanghai Jiaotong University, Shanghai 200080, People's Republic of China

S *Supporting Information*

ABSTRACT: Chlorotoxin-conjugated multifunctional dendrimers labeled with radionuclide ^{131}I were synthesized and utilized for targeted single photon emission computed tomography (SPECT) imaging and radiotherapy of cancer. In this study, generation five amine-terminated poly(amidoamine) dendrimers were used as a platform to be sequentially conjugated with polyethylene glycol (PEG), targeting agent chlorotoxin (CTX), and 3-(4′-hydroxyphenyl)propionic acid-OSu (HPAO). This was followed by acetylation of the remaining dendrimer terminal amines and radiolabeling with ^{131}I to form the targeted theranostic dendrimeric nanoplatform. We show that the dendrimer platform possessing approximately 7.7 CTX and 21.1 HPAO moieties on each dendrimer displays excellent cytocompatibility in a given concentration range (0−20 μM) and can specifically target cancer cells overexpressing matrix metallopeptidase 2 (MMP2) due to the attached CTX. With the attached HPAO moiety having the phenol group, the dendrimer platform can be effectively labeled with radioactive ^{131}I with good stability and high radiochemical purity. Importantly, the ^{131}I labeling renders the dendrimer platform with an ability to be used for targeted SPECT imaging and radiotherapy of an MMP2-overexpressing glioma model *in vivo*. The developed radiolabeled multifunctional dendrimeric nanoplatform may hold great promise to be used for targeted theranostics of human gliomas.

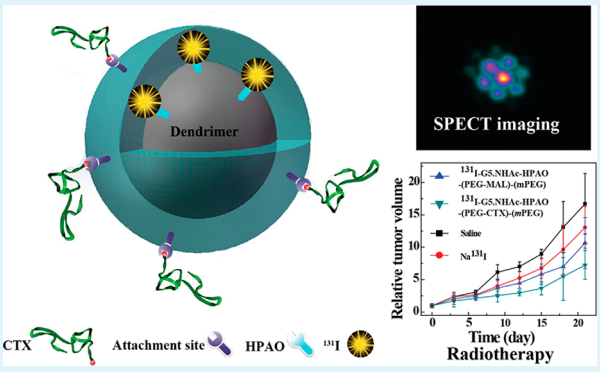

KEYWORDS: *dendrimers, chlorotoxin, glioma, SPECT imaging, radiotherapy*

INTRODUCTION

Cancer therapy remains a tremendous global challenge.[1−4] Current cancer treatments include surgery, radiation therapy, and chemotherapy, but these fail to significantly improve the survival rates of cancer patients.[5−8] In recent years, nanotechnology has revolutionized cancer therapy with extensive prospects for clinical applications.[6−9] Nanotechnology can not only provide precise cancer imaging information for surgical excision but also develop novel platforms for cancer therapy.[9] For instance, various nanoparticulate systems have been designed for noninvasive imaging applications such as fluorescence imaging,[10,11] magnetic resonance (MR) imaging,[12,13] and computed tomography (CT).[14,15] Likewise, a variety of nanocarrier systems have also been developed to load chemotherapeutic agents or genes for cancer therapy in order to maximize the therapeutic efficacy with minimal damage to normal tissues.[16−18] Importantly, some researchers have developed novel theranostic nanoplatforms that combine the diagnostic and therapeutic functions for cancer treatment.[19−21]

Nuclear medicine utilizes radionuclides and radiolabeled compounds to diagnose and treat diseases, playing an increasingly important role in medical sciences.[22−27] With the development of nuclear medicine, radionuclide imaging and radiotherapy of cancer have been the focus of basic research and clinical practice.[22−28] Radionuclide-based imaging techniques such as single photon emission computed tomography

Received: June 30, 2015
Accepted: August 20, 2015
Published: August 20, 2015

DOI: 10.1021/acsami.5b05836
ACS Appl. Mater. Interfaces 2015, 7, 19798−19808

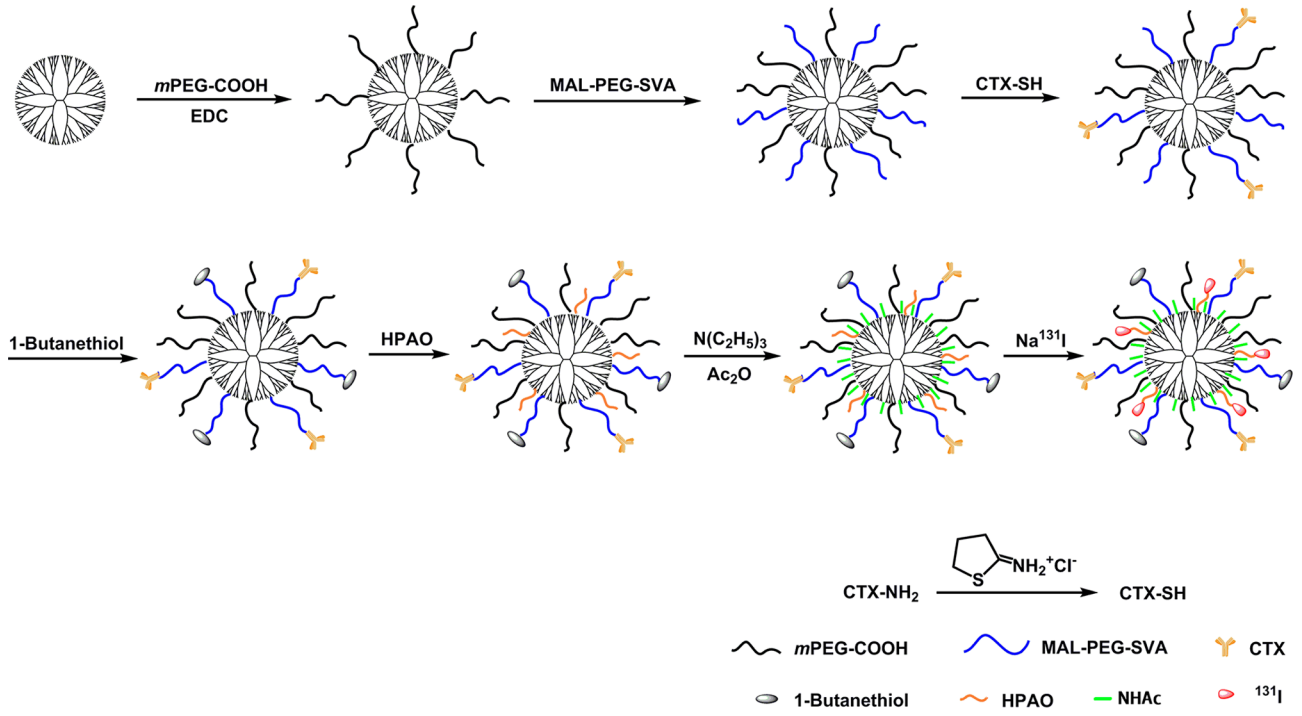

Figure 1. Schematic illustration of the synthesis of the ^{131}I-G5.NHAc-HPAO-(PEG-CTX)-(*m*PEG) dendrimers. Ac_2O represents acetic anhydride.

(SPECT) and positron emission tomography (PET), unlike CT and MR imaging, are highly sensitive and quantitative in diagnosis.[28] In clinical applications, technetium-99m (^{99m}Tc) and iodine-131 (^{131}I) are mostly used for SPECT imaging,[29] while fluorine-18 (^{18}F) and carbon-11 (^{11}C) are widely applied for PET imaging.[30] Concurrently, radiotherapy that delivers cytotoxic levels of energy from radionuclides to disease sites has been used to treat various tumors.[31,32] Many radionuclides including ^{131}I,[31] phosphorus-32 (^{32}P),[31] strontium-89 (^{89}Sr),[33] yittrium-90 (^{90}Y),[34] and rhenium-188 (^{188}Re)[31] have been applied for radiotherapy in the clinic. Among these, ^{131}I has been received considerable attention because of its relative long half-life ($t_{1/2}$ = 8.01 days), appropriate radiation energy (0.606 MeV, 89.9%), and convenient labeling methods.[31−34] Furthermore, ^{131}I has also been used for SPECT imaging, enabling simultaneous radionuclide imaging and radiotherapy.[35−37] However, because of the specific affinity of free ^{131}I for the thyroid, free ^{131}I is difficult to directly accumulate within the tumor site to achieve effective SPECT imaging and radiotherapy. Thus, it is critical to select an appropriate carrier system to specifically deliver ^{131}I to the tumor site.

Poly(amidoamine) (PAMAM) dendrimers are a class of highly symmetric, branched, monodispersed synthetic macromolecules that have been widely investigated as a platform for cancer imaging[12,38] and therapy.[39−41] In the past decades, many researchers have shown that anticancer drugs or therapeutic genes can be carried by dendrimers for cancer therapy applications.[42−46] Dendrimers can also be attached with targeting ligands and contrast agents for targeted cancer imaging.[47−53] Recent studies have demonstrated that dendrimers conjugated with radionuclides can be used for cancer imaging;[54−56] however, the therapeutic potential of the dendrimer conjugates has not been fully explored.

On the basis of the inherent SPECT imaging and radiotherapy properties of ^{131}I and the versatile dendrimer nanotechnology, we attempted to develop a dendrimer-based theranostic platform for targeted tumor SPECT imaging and radiotherapy. In this study, amine-terminated poly(amidoamine) (PAMAM) dendrimers of generation 5 (G5.NH_2) were sequentially conjugated with polyethylene glycol (PEG), targeting ligand chlorotoxin (CTX), and 3-(4′-hydroxyphenyl)propionic acid-OSu (HPAO), followed by acetylation of the remaining terminal amines of dendrimers and radiolabeling with ^{131}I to form the targeted theranostic nanoplatform of ^{131}I-G5.NHAc-HPAO-(PEG-CTX)-(*m*PEG) (Figure 1). The unlabeled and labeled multifunctional dendrimers were characterized via different techniques. The cytotoxicity of the unlabeled dendrimers (G5.NHAc-HPAO-(PEG-CTX)-(*m*PEG)) was assessed *via in vitro* cell viability assay. Flow cytometry and confocal microscopy were used to evaluate the binding specificity of the G5.NHAc-HPAO-(PEG-CTX)-(*m*PEG) dendrimers toward cancer cells overexpressing matrix metallopeptidase 2 (MMP2). To evaluate the stability of the ^{131}I-G5.NHAc-HPAO-(PEG-CTX)-(*m*PEG) dendrimers, the radiochemical purity at different time points was analyzed. Finally, the resulting ^{131}I-G5.NHAc-HPAO-(PEG-CTX)-(*m*PEG) dendrimers were used as a platform for targeted SPECT imaging and radiotherapy of a MMP2-overexpressing glioma model *in vivo*.

EXPERIMENTAL SECTION

Materials. G5.NH_2 PAMAM dendrimers with an ethylenediamine core and polydispersity index less than 1.08 were from Dendritech (Midland, MI). PEG with one end of maleimide group and the other end of succinimidyl valerate group (MAL-PEG-SVA, Mw = 5000) and PEG monomethyl ether with a carboxyl end group (*m*PEG-COOH, Mw = 5000) were provided by Shanghai Yanyi Biotechnology Corporation (Shanghai, China). Na^{131}I was obtained from Shanghai GMS Pharmaceutical Co., Ltd. (Shanghai, China). Chloramine-T trihydrate (ch-T), potassium iodide (KI), 1-butanethiol, sodium metabisulfite ($Na_2S_2O_5$), and HPAO were from J&K Chemical Ltd. (Shanghai, China). CTX was from Chinese Peptide Company (Hangzhou, China). 2-Iminothiolane hydrochloride, 3-(4,5-dime-

DOI: 10.1021/acsami.5b05836
ACS Appl. Mater. Interfaces 2015, 7, 19798−19808

thylthiazol-2-yl)-2,5-diphenyltetrazolium bromide (MTT), acetic anhydride, triethylamine, 1-ethyl-3-(3-(dimethylamino)propyl) carbodiimide hydrochloride (EDC), and all the other chemicals and solvents were provided from Aldrich (St. Louis, MO). Disposable PD-10 desalting columns were from GE Pharmacia (GE Inc., Fairfield, CT). C6 cells (a rat glioma cell line) and L929 cells (a mouse fibroblast cell line) were purchased from Institute of Biochemistry and Cell Biology (The Chinese Academy of Sciences, Shanghai, China). Dulbecco's Modified Eagle's Medium (DMEM), fetal bovine serum (FBS), penicillin, and streptomycin were from Hangzhou Jinuo Biomedical Technology (Hangzhou, China). Water used in all experiments was purified by a Milli-Q Plus 185 water purification system (Millipore, Bedford, MA) with a resistivity above 18 MΩ cm. Regenerated cellulose dialysis membranes (molecular weight cutoff, MWCO = 14 000 and 1 000) were provided from Fisher (Pittsburgh, PA).

Synthesis of the G5.NHAc-HPAO-(PEG-CTX)-(*m*PEG) Dendrimers. We synthesized CTX-conjugated dendrimers according to the literature.[57,58] Briefly, CTX-NH_2 (2 mg, 0.0005 mmol) dissolved in 5 mL of DMSO was reacted with 2 mol equiv of 2-iminothiolane hydrochloride (0.14 mg, 0.001 mmol) in 2 mL of DMSO at room temperature for 24 h with stirring. The reaction mixture was extensively dialyzed against phosphate buffered saline (PBS, 3 times, 4 L) and water (3 times, 4 L) through a dialysis membrane with an MWCO of 1 000 for 3 days to remove the excess reactants. The obtained CTX-SH solution in dialysis liquid was then collected.

*m*PEG-COOH (144.2 mg, 5 mL DMSO) with 15 mol equiv of G5.NH_2 (50.0 mg, 5 mL of DMSO) was first activated by EDC (110.6 mg, 5 mL of DMSO) and then reacted with the DMSO solution of G5.NH_2 under vigorous magnetic stirring for 3 days to acquire the raw G5.NH_2-*m*PEG dendrimers. Then, MAL-PEG-SVA (144.2 mg, 5 mL of DMSO) with 15 mol equiv of G5.NH_2 was dropwise added into the G5.NH_2-*m*PEG dendrimer solution under stirring for 3 days. The formed G5.NH_2-(PEG-MAL)-(*m*PEG) dendrimers in DMSO solution were mixed with the above CTX-SH solution under vigorous magnetic stirring for 24 h to get the G5.NH_2-(PEG-CTX)-(*m*PEG) dendrimers. To avoid the remaining maleimide groups of PEG-MAL conjugated onto the surface of dendrimers to react with HPAO added in the following reaction (see below), we used excess 1-butanethiol (15.5 μL, 5 mol equiv of PEG-MAL) to react with the remaining maleimide groups on the surface of the dendrimers under vigorous stirring for 24 h.

Then, HPAO (15.2 mg, 5 mL of DMSO) with 30 mol equiv of G5.NH_2 was mixed with the DMSO solution of the G5.NH_2-(PEG-CTX)-(*m*PEG) dendrimers under stirring. The reaction was stopped after 24 h to obtain the raw G5.NH_2-HPAO-(PEG-CTX)-(*m*PEG) conjugates. After that, excess triethylamine (178.4 μL) was added to the G5.NH_2-HPAO-(PEG-CTX)-(*m*PEG) conjugate solution and the mixture was thoroughly stirred for 30 min. Acetic anhydride (100.9 μL) with 5 mol equiv of the dendrimer terminal amines was then dropwise added into the above dendrimer/triethylamine mixture solution under stirring for 24 h. Finally, the reaction mixture was purified via dialysis with a similar procedure to that used to purify CTX-SH to get the G5.NHAc-HPAO-(PEG-CTX)-(*m*PEG) dendrimers except the use of a dialysis membrane with an MWCO 14 000, followed by lyophilization to get the product of G5.NHAc-HPAO-(PEG-CTX)-(*m*PEG) dendrimers. For comparison, G5.NHAc-HPAO-(PEG-MAL)-(*m*PEG) dendrimers without CTX were also synthesized.

Synthesis of the ^{131}I-G5.NHAc-HPAO-(PEG-CTX)-(*m*PEG) Dendrimers. We labeled ^{131}I to the G5.NHAc-HPAO-(PEG-CTX)-(*m*PEG) dendrimers through the phenol group of the HPAO moiety according to protocols described in the literature.[59,60] Briefly, sterile Na^{131}I solution (185−370 MBq, 0.5−1 mL) was added to a vial containing the G5.NHAc-HPAO-(PEG-CTX)-(*m*PEG) dendrimer (200 μg) and the ch-T (100 μg) codissolved in 200 μL of PBS (0.1 M, pH = 7.2−7.4) with continuous stirring. The reaction mixture was incubated at room temperature for 2 min before $Na_2S_2O_5$ (100 μg) was added to terminate the reaction. The final reaction mixture was then eluted with a PD-10 desalting column and 1 mL of liquid was collected in each tube. After 20 tubes were collected, the radioactivity of each aliquot tube was measured with a CRC-15R radioisotope dose calibrator (Capintec, Inc., Ramsey, NJ). Through the same method, we also labeled ^{131}I on the surface of the control device of G5.NHAc-HPAO-(PEG-MAL)-(*m*PEG) dendrimer under similar experimental conditions.

Characterization Techniques. ^{1}H NMR spectra were obtained on a Bruker AV-400 NMR spectrometer. All samples prior to the ^{131}I labeling were prepared in D_2O before measurements. Zeta potential and dynamic light scattering (DLS) measurements were conducted using a Malvern Zetasizer (Nano ZS model ZEN3600, Worcestershire, U.K.) equipped with a standard 633 nm laser. Dendrimers were dissolved in water at a concentration of 1 mg/mL before measurements.

Radiochemical Purity Analysis. The radiochemical purity of the ^{131}I-G5.NHAc-HPAO-(PEG-CTX)-(*m*PEG) and ^{131}I-G5.NHAc-HPAO-(PEG-MAL)-(*m*PEG) dendrimers was analyzed by instant thin-layer chromatography (ITLC) using silica gel-coated fiber glass sheets (Macherey-Nagel, GmbH & Co. KG, Düren, Germany). Saline was utilized as the mobile phase, and the sheets were analyzed with a thin-layer chromatogram scanner (Bioscan Inc., Tucson, AZ).

***In Vitro* Radiolabeling Stability Study.** The stability of the radiolabeled ^{131}I-G5.NHAc-HPAO-(PEG-CTX)-(*m*PEG) and ^{131}I-G5.NHAc-HPAO-(PEG-MAL)-(*m*PEG) dendrimers *in vitro* was studied by measuring the radiochemical purity via ITLC at different time intervals.[60] Briefly, the ^{131}I-G5.NHAc-HPAO-(PEG-CTX)-(*m*PEG) dendrimers (100 μL, 18.5 MBq) or ^{131}I-G5.NHAc-HPAO-(PEG-MAL)-(*m*PEG) dendrimers (100 μL, 18.5 MBq) were mixed with 1 mL of PBS at room temperature. ITLC was then utilized to analyze the radiochemical purity of the ^{131}I-G5.NHAc-HPAO-(PEG-CTX)-(*m*PEG) or ^{131}I-G5.NHAc-HPAO-(PEG-MAL)-(*m*PEG) dendrimers after incubation at room temperature for 1, 6, and 24 h, respectively. A similar procedure was applied to evaluate the radiochemical stability of the dendrimers in FBS at 37 °C.

Cell Culture. We cultured C6 and L929 cells continuously in 25 cm^2 tissue culture flasks with 5 mL of DMEM containing 10% FBS, 100 U/mL penicillin, and 100 U/mL streptomycin in a humidified incubator with 5% CO_2 at 37 °C.

***In Vitro* Cytotoxicity Assay and Cell Morphology Observation.** MTT assay was used to assess the cytotoxicity of the G5.NHAc-HPAO-(PEG-CTX)-(*m*PEG) dendrimers *in vitro*. Briefly, C6 cells (1×10^4) were seeded into each well of a 96-well plate. After 24 h to bring the cells to confluence, the medium was removed and 200 μL of fresh medium containing the G5.NHAc-HPAO-(PEG-CTX)-(*m*PEG) dendrimers with different concentrations was added into each well. After 24 h incubation at 37 °C, an MTT solution (5 mg/mL, 20 μL in PBS) was added to each well. After another 4 h incubation at 37 °C, the medium in each well was replaced with DMSO (200 μL) to dissolve the formazan crystals. The absorbance was measured at 570 nm using a Thermo Scientific Multiskan MK3 ELISA reader (Thermo Scientific, Waltham, MA) according to the manufacturer's instructions. For comparison, a similar procedure was applied to evaluate the cytotoxicity of the G5.NHAc-HPAO-(PEG-CTX)-(*m*PEG) dendrimers with a normal cell line (L929 cells). We calculated the mean and standard deviation of triplicate wells for each sample. The cell morphology was also observed with a Leica DM IL LED inverted phase contrast microscope after treatment with the G5.NHAc-HPAO-(PEG-CTX)-(*m*PEG) dendrimers at different concentrations for 24 h.

Flow Cytometry Analysis. Here we synthesized fluorescein isothiocyanate (FI)-modified dendrimers (G5.NHAc-FI-HPAO-(PEG-CTX)-(*m*PEG)) with the same modifications of *m*PEG, PEG-CTX, HAPO, and acetylation as those of the G5.NHAc-HPAO-(PEG-CTX)-(*m*PEG) dendrimers. The targeting efficiency of the G5.NHAc-HPAO-(PEG-CTX)-(*m*PEG) dendrimers toward C6 cells was assessed by flow cytometry.[53] Briefly, 2×10^5 C6 cells were first seeded into each well of a 12-well plate. After overnight incubation, the medium was replaced with 1 mL of fresh DMEM containing the G5.NHAc-FI-HPAO-(PEG-MAL)-(*m*PEG) or G5.NHAc-FI-HPAO-(PEG-CTX)-(*m*PEG) dendrimers at the ultimate concentrations of 0.4 μM and 4 μM, respectively. After 2 h, the cells were trypsinized, resuspended in PBS containing 0.1% bovine serum albumin, and

DOI: 10.1021/acsami.5b05836
ACS Appl. Mater. Interfaces 2015, 7, 19798−19808

measured using a Becton Dickinson FACScan analyzer. For comparison, we also evaluated the cellular uptake of the G5.NHAc-FI-HPAO-(PEG-MAL)-(*m*PEG) and G5.NHAc-FI-HPAO-(PEG-CTX)-(*m*PEG) dendrimers with cells having no MMP2 expression (L929 cells) under similar experimental conditions. Approximately 10 000 cells were recorded in the FL1-fluorescence channel, and the mean fluorescence of the gated viable cells was analyzed.

Confocal Microscopy. The cellular uptake of the G5.NHAc-FI-HPAO-(PEG-CTX)-(*m*PEG) dendrimers by C6 cells was observed with confocal microscopy (Carl Zeiss LSM 700, Jena, Germany). Briefly, coverslips were pretreated according to our previous work.[61] Then, C6 cells (5×10^4) were seeded into each well of a 12-well plate and cultured overnight to allow the cells to attach onto the coverslips. The medium was then replaced with 1 mL of fresh medium containing PBS (control), G5.NHAc-FI-HPAO-(PEG-MAL)-(*m*PEG) dendrimers (0.4 μM and 4 μM), and G5.NHAc-FI-HPAO-(PEG-CTX)-(*m*PEG) dendrimers (0.4 μM and 4 μM), respectively. The cells were incubated at 37 °C and 5% CO_2 for 2 h, rinsed with PBS, fixed with glutaraldehyde (2.5%) at 4 °C for 15 min, and then counterstained with Hoechst 33342 (1 μg/mL) at 37 °C for 20 min according to a standard procedure. The FI fluorescence was excited with a 488 nm argon blue laser and a 505−525 nm barrier filter was applied to collect the FI emission. Samples were scanned using a 63× oil-immersion objective lens, and the optical section thickness was set at 5 mm.

Targeted SPECT Imaging of Glioma *in Vivo*. Animal experiments were approved by the ethical committee of Shanghai General Hospital. For *in vivo* imaging experiments, 6-week-old BALB/c female nude mice (21−23 g, Shanghai Slac Laboratory Animal Center, Shanghai, China) were inoculated subcutaneously with 2×10^6 C6 cells/mouse in the right side of flank. At approximately 3 weeks postinjection, the tumors reached a volume of 0.5−1.0 cm^3. These mice were fed with water containing 1% potassium iodide for 7 days before SPECT imaging to decrease the thyroid uptake of the ^{131}I-labeled dendrimers or ^{131}I ions. The mice were randomly divided into the experimental and control groups. We then intravenously injected a PBS solution of the ^{131}I-G5.NHAc-HPAO-(PEG-CTX)-(*m*PEG) dendrimers ([^{131}I] = 92.5 MBq/mL, 200 μL) to the mice via tail vein. For comparison, nontargeted ^{131}I-G5.NHAc-HPAO-(PEG-MAL)-(*m*PEG) dendrimers without CTX were also injected at the same dose. Before SPECT imaging, all mice were anesthetized with pentobarbital sodium (40 mg/kg).

SPECT images were acquired at 5 min, 30 min, 1 h, 2 h, 4 h, 6 h, 15 h, and 24 h postinjection using an Infinia SPECT scanner equipped with an Xeleris Workstation and High Energy General Purpose collimator (GE Inc., Fairfield, CT). At 15 h postinjection, one mouse of each experimental group was sacrificed. The major organs and tumors were removed and their relative radioactivity ratios were recorded by analyzing the regions of interest.

Targeted Tumor Radiotherapy *in Vivo*. The mice were randomized into six different groups and numbered after the glioma model was established. A PBS solution of the ^{131}I-G5.NHAc-HPAO-(PEG-CTX)-(*m*PEG) dendrimers ([^{131}I] = 37 MBq/mL, 200 μL) was intravenously injected into each mouse in the first group via the tail vein every third day. For comparison, saline (200 μL), G5.NHAc-HPAO-(PEG-MAL)-(*m*PEG) dendrimers (200 μL), G5.NHAc-HPAO-(PEG-CTX)-(*m*PEG) dendrimers (200 μL), Na^{131}I solution (200 μL), and ^{131}I-G5.NHAc-HPAO-(PEG-MAL)-(*m*PEG) dendrimers with the same concentration of the ^{131}I-G5.NHAc-HPAO-(PEG-CTX)-(*m*PEG) dendrimers were injected. Mice in all groups were injected for a total of seven times. Three days after each injection, the tumor size and the body weight of each mouse were recorded at predetermined time points. During the treatment period, we recorded the mouse death to get the survival rate. The tumor inhibition efficacy was finally evaluated according to protocols described in our previous work.[61]

H&E Staining. After seven injection treatments for a period of 21 days, mice treated with saline, Na^{131}I, G5.NHAc-HPAO-(PEG-MAL)-(*m*PEG), G5.NHAc-HPAO-(PEG-CTX)-(*m*PEG), ^{131}I-G5.NHAc-HPAO-(PEG-MAL)-(*m*PEG), and ^{131}I-G5.NHAc-HPAO-(PEG-CTX)-(*m*PEG) were sacrificed and the tumors and major organs (heart, liver, spleen, lung, and kidney) were extracted. According to the standard procedure of hematoxylin and eosin (H&E) staining, the tumors and organs were fixed with 10% neutral buffered formalin, embedded in paraffin, sectioned into 4-μm thick slices, and then stained with H&E. Finally, the sections were observed using a Leica DM IL LED inverted phase contrast microscope.

TUNEL Assay. The tumor tissue apoptosis of each group of mice was further studied using a terminal deoxynucleotidyl transferase dUTP nick end labeling (TUNEL) method by apoptotic detection kit (Roche, Basel, Switzerland) according to the literature.[61] Through the treatments of fixation, dehydration, paraffin-embedment, sectioning, and staining using a TUNEL kit, the tumor sections were finally observed with a Leica DM IL LED inverted phase contrast microscope. The number of TUNEL-positive cells was counted from five random fields for each tumor section.

Statistical Analysis. The significance of the experimental data was assessed by one-way ANOVA statistical analysis method. A value of 0.05 was considered to be significant, and the data were marked with (*) for $p < 0.05$, (**) for $p < 0.01$, and (***) for $p < 0.001$, respectively.

RESULTS AND DISCUSSION

Synthesis and Characterization of the ^{131}I-G5.NHAc-HPAO-(PEG-CTX)-(*m*PEG) Dendrimer. Radioactive ^{131}I-labeled multifunctional G5.NHAc-HPAO-(PEG-CTX)-(*m*PEG) dendrimers were synthesized for targeted tumor SPECT imaging and radiotherapy. In this study, amine-terminated G5 PAMAM dendrimers were sequentially conjugated with *m*PEG-COOH, PEG-CTX, and HPAO, followed by acetylation of the remaining dendrimer terminal amines and labeling of radioactive ^{131}I (Figure 1). Detail molecular structure of the CTX-conjugated multifunctional dendrimers labeled with ^{131}I can be seen in Figure S1 (Supporting Information).

CTX was selected to be conjugated onto the dendrimer surface in order to specifically target MMP2-overexpressing cancer cells,[57,58,62] while HPAO attached onto the dendrimer surface was used for ^{131}I labeling through the phenol group of HPAO.[60] The formed ^{131}I-G5.NHAc-HPAO-(PEG-CTX)-(*m*PEG) dendrimers were characterized by different methods.

The conjugation of *m*PEG-COOH onto the surface of G5.NH_2 dendrimers was characterized via ^{1}H NMR. On the basis of the characteristic peaks at 3.4−3.6 ppm corresponding to 448 protons of repeating $-CH_2CH_2O-$ groups of *m*PEG-COOH, the number of *m*PEG-COOH conjugated onto each G5 dendrimer was calculated to be 11.2 (Figure S2, Supporting Information). Then the heterofunctional MAL-PEG-SVA was attached to the G5 dendrimer surface. Through the NMR integration, the number of PEG-MAL conjugated onto each G5 dendrimer was estimated to be 8.4 (Figure S3, Supporting Information). Followed by thiol-maleimide coupling, thiolated CTX was conjugated onto the dendrimer surface. The number of CTX attached to each G5 dendrimer was estimated to be 7.7 by integration of the characteristic peaks at 1.0−1.5 ppm associated with 52 protons of CTX (Figure S4, Supporting Information). Further, HPAO was modified onto the surface of G5 dendrimers for ^{131}I labeling. By integration of the characteristic peaks at 6.6 and 6.9 ppm associated with the four protons on the HPAO phenol, the number of the HPAO moieties modified onto each dendrimer was estimated to be 21.1 (Figure S5, Supporting Information). The control device of the G5.NHAc-HPAO-(PEG-MAL)-(*m*PEG) dendrimer without CTX was also characterized. The practical numbers of *m*PEG and PEG-MAL attached to each G5 dendrimer were comparable to those of the targeted G5.NHAc-HPAO-(PEG-

DOI: 10.1021/acsami.5b05836
ACS Appl. Mater. Interfaces 2015, 7, 19798−19808

CTX)-(*m*PEG) dendrimer (Figure S6, Supporting Information). Zeta potential measurements were used to examine the surface potential of the multifunctional dendrimers (Table S1, Supporting Information). The surface potential of the G5.NHAc-HPAO-(PEG-CTX)-(*m*PEG) and G5.NHAc-HPAO-(PEG-MAL)-(*m*PEG) dendrimers are +25.9 and +27.9 mV, respectively. DLS was used to measure the hydrodynamic size of the multifunctional dendrimers (Table S1, Supporting Information), and the hydrodynamic sizes of the G5.NHAc-HPAO-(PEG-CTX)-(*m*PEG) and G5.NHAc-HPAO-(PEG-MAL)-(*m*PEG) dendrimers are 233.5 and 256.1 nm, respectively. The relatively large hydrodynamic size of the dendrimers could be due to the PEG modification, slightly enhancing the interdendrimer interaction via hydrogen bonding. In any case, their hydrodynamic size distribution is relatively narrow with a quite low polydispersity index.

Finally, ^{131}I-G5.NHAc-HPAO-(PEG-CTX)-(*m*PEG) dendrimers were successfully prepared with the optimized yields by the ch-T method. Quality control tests using ITLC chromatography demonstrated a single peak (Rf value = 0.1−0.2) for the ^{131}I-G5.NHAc-HPAO-(PEG-CTX)-(*m*PEG) dendrimer, and the product had a relative high radiochemical purity (98.4% ± 0.8%).

Radiostability of the ^{131}I-G5.NHAc-HPAO-(PEG-CTX)-(*m*PEG) Dendrimer. For SPECT imaging and radiotherapy applications, the radiostability of the ^{131}I-G5.NHAc-HPAO-(PEG-CTX)-(*m*PEG) dendrimer (Figure S7, Supporting Information) and the ^{131}I-G5.NHAc-HPAO-(PEG-MAL)-(*m*PEG) dendrimer (Figure S8, Supporting Information) was first investigated. *In vitro* radiostability assay data reveal that both ^{131}I-G5.NHAc-HPAO-(PEG-CTX)-(*m*PEG) and ^{131}I-G5.NHAc-HPAO-(PEG-MAL)-(*m*PEG) dendrimers have satisfactory stability within 24 h *in vitro* after exposure to PBS or FBS solution, and at least 90% of the ^{131}I labeled dendrimers still keep the original structure without free ^{131}I separation from the dendrimer backbones (Table S2, Supporting Information). This suggests that the ^{131}I labeling onto the dendrimer is pretty stable, ensuring the further *in vivo* radionuclide imaging and radiotherapy applications.

Cytocompatibility. The cytocompatibility of the G5.NHAc-HPAO-(PEG-CTX)-(*m*PEG) dendrimers before ^{131}I labeling was assessed by MTT cell viability assay of C6 (Figure 2) and L929 cells (Figure S9, Supporting Information). We can see that C6 cells display a relative high viability (>90%) after treatment with the G5.NHAc-HPAO-(PEG-CTX)-(*m*PEG) dendrimers at the concentration up to 20 μM, which is comparable to the control cells treated with PBS. Likewise, similar results can be observed in the MTT cell viability assay of normal L929 cells, further indicating that the formed G5.NHAc-HPAO-(PEG-CTX)-(*m*PEG) dendrimers have no cytotoxicity toward normal cells in the studied concentration range. The good cytocompatibility of the dendrimers can be further confirmed by observation of the morphology of C6 cells (Figure S10, Supporting Information). C6 cells treated with the G5.NHAc-HPAO-(PEG-CTX)-(*m*PEG) dendrimers at different concentrations (0.1 μM, 1 μM, 5 μM, 10 μM, and 20 μM, respectively) for 24 h are adherent and healthy, similar to the control cells treated with PBS. Taken together, both quantitative MTT assay data and qualitative cell morphology observation suggest that the developed G5.NHAc-HPAO-(PEG-CTX)-(*m*PEG) dendrimers are cytocompatible in the given concentration range.

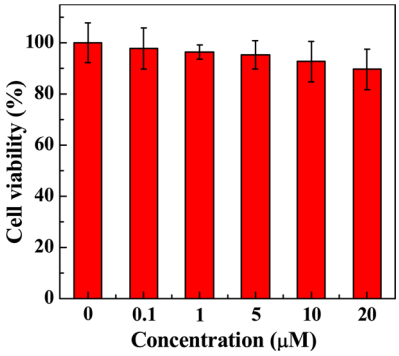

Figure 2. MTT assay of C6 cell viability after treatment with the G5.NHAc-HPAO-(PEG-CTX)-(*m*PEG) dendrimers at different concentrations for 24 h.

Targeting Specificity of the G5.NHAc-HPAO-(PEG-CTX)-(*m*PEG) Dendrimer. CTX is known to bind to functional proteins like MMP2 and chloride ion channels,[57,58,62] and MMP2 is known to be overexpressed in glioma, medulloblastoma, prostate cancer, sarcoma, and intestinal cancer.[58,63] Thus, the prepared G5.NHAc-HPAO-(PEG-CTX)-(*m*PEG) dendrimers are expected to be able to specifically bind to MMP2-overexpressing cancer cells. The conjugation of FI onto the dendrimers enabled us to analyze the cellular uptake of the G5.NHAc-FI-HPAO-(PEG-CTX)-(*m*PEG) dendrimers by flow cytometry (Figure 3) and confocal microscopy (Figure 4). Through quantitative analysis of the ^{1}H NMR spectra, the number of FI moiety modified onto each dendrimer was calculated to be 6.3 and 6.8 for the G5.NHAc-FI-HPAO-(PEG-CTX)-(*m*PEG) and G5.NHAc-FI-HPAO-(PEG-MAL)-(*m*PEG) dendrimers, respectively (Figure S11, Supporting Information).

From the flow cytometric analysis, we can clearly see that C6 cells treated with the G5.NHAc-FI-HPAO-(PEG-CTX)-(*m*PEG) dendrimers for 2 h display significantly higher fluorescence intensity than those treated with the G5.NHAc-FI-HPAO-(PEG-MAL)-(*m*PEG) dendrimers without CTX (Figure 3b−f). The C6 cells treated with the G5.NHAc-FI-HPAO-(PEG-MAL)-(*m*PEG) dendrimers without CTX exhibit similar fluorescence intensity to those treated with PBS (Figures 3b,d,f). These data confirm that the G5.NHAc-FI-HPAO-(PEG-CTX)-(*m*PEG) dendrimers are able to specifically target C6 cells presumably through specific MMP2-CTX interaction, in agreement with the literature.[57,62] In order to further prove the binding specificity of the G5.NHAc-FI-HPAO-(PEG-CTX)-(*m*PEG) dendrimers to MMP2-overexpressing C6 cells, normal L929 cells without MMP2-expression were also tested under similar experimental conditions. Clearly, the fluorescence intensity of L929 cells treated with the G5.NHAc-FI-HPAO-(PEG-CTX)-(*m*PEG) or G5.NHAc-FI-HPAO-(PEG-MAL)-(*m*PEG) dendrimers at 4 μM displays no significant differences and is much lower than that of C6 cells treated with the G5.NHAc-FI-HPAO-(PEG-CTX)-(*m*PEG) dendrimers at the same concentration (4 μM) ($p < 0.001$, Figure 3f).

Confocal microscopy was also used to demonstrate the targeting specificity of the formed G5.NHAc-FI-HPAO-(PEG-CTX)-(*m*PEG) dendrimers (Figure 4). After 2 h treatment with the G5.NHAc-FI-HPAO-(PEG-CTX)-(*m*PEG) dendrimers (0.4 μM, 4 μM), C6 cells display much stronger fluorescence signals than those treated with the control

DOI: 10.1021/acsami.5b05836
ACS Appl. Mater. Interfaces 2015, 7, 19798−19808

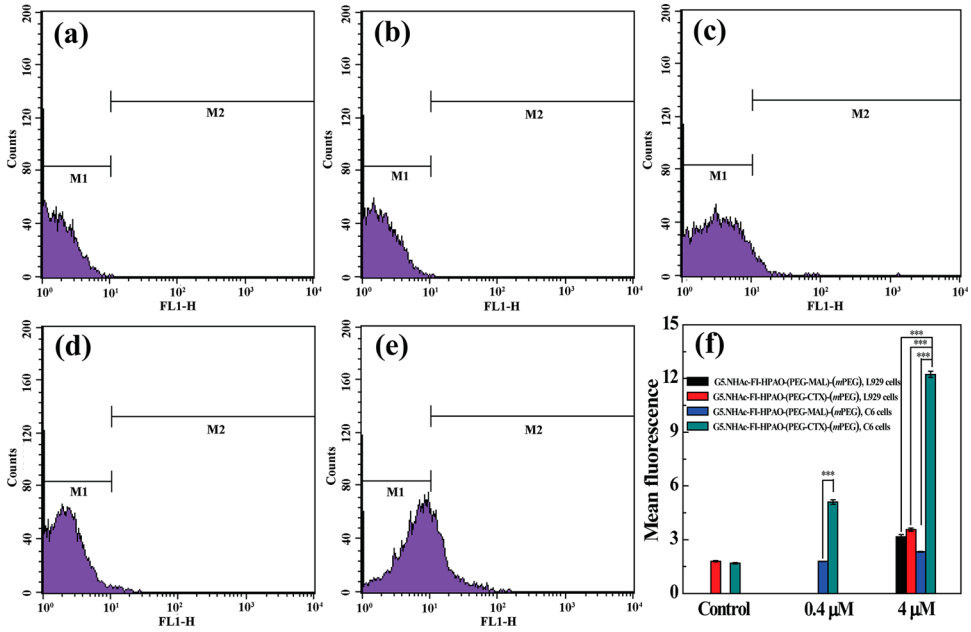

Figure 3. Flow cytometric analysis of C6 cells treated with PBS (a), the G5.NHAc-FI-HPAO-(PEG-MAL)-(*m*PEG) dendrimers at 0.4 μM (b) and 4 μM (d), and the G5.NHAc-FI-HPAO-(PEG-CTX)-(*m*PEG) dendrimers at 0.4 μM (c) and 4 μM (e) for 2 h, respectively. Part f shows the comparison of the binding of different dendrimers with L929 and C6 cells.

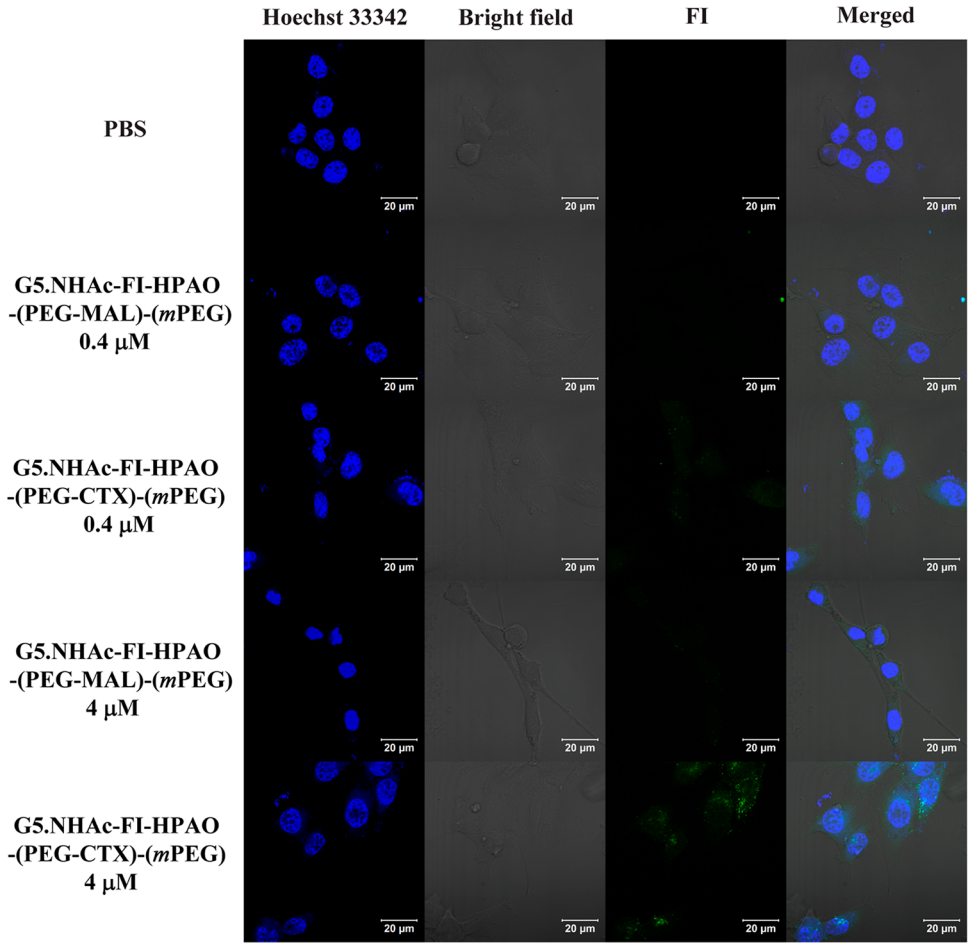

Figure 4. Confocal microscopy images of C6 cells treated with the G5.NHAc-FI-HPAO-(PEG-MAL)-(*m*PEG) or G5.NHAc-FI-HPAO-(PEG-CTX)-(*m*PEG) dendrimers with different concentrations for 2 h, respectively.

DOI: 10.1021/acsami.5b05836
ACS Appl. Mater. Interfaces 2015, 7, 19798−19808

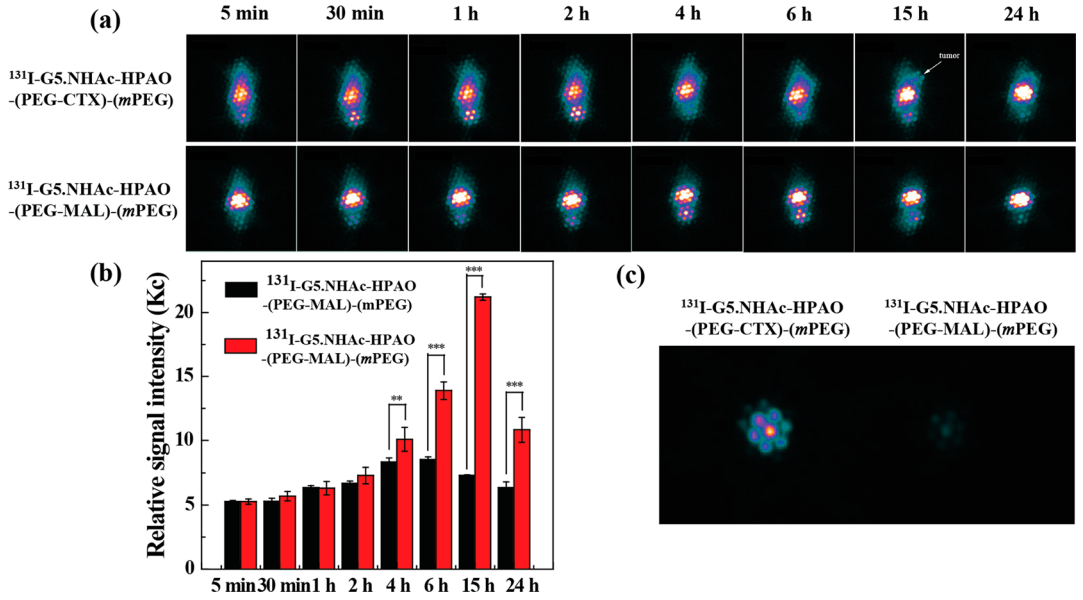

Figure 5. SPECT images of the nude mice bearing C6 xenografted tumors (a) and the relative SPECT signal intensities of tumors (b) at different time points post intravenous injection of the ^{131}I-G5.NHAc-HPAO-(PEG-CTX)-(*m*PEG) and ^{131}I-G5.NHAc-HPAO-(PEG-MAL)-(*m*PEG) dendrimers. Part c shows the SPECT images of *ex vivo* tumors after the corresponding treatments for 15 h.

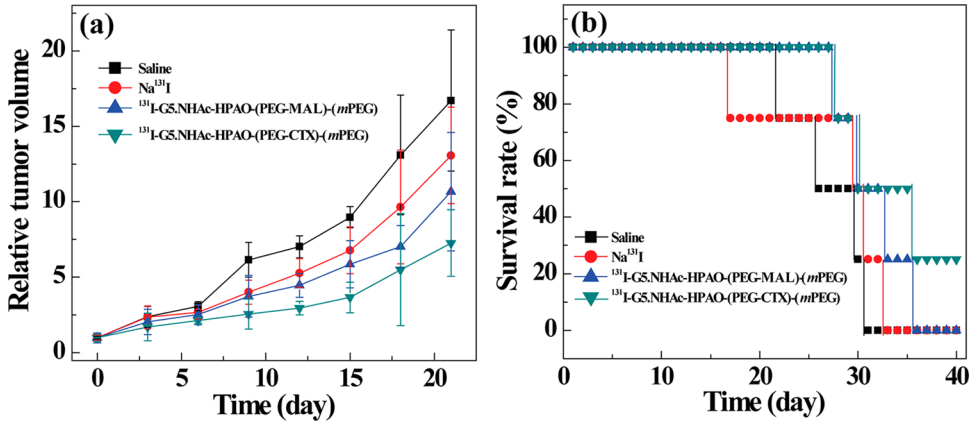

Figure 6. (a) Growth of C6 xenografted tumors after various treatments. The relative tumor volume was normalized according to their initial tumor volume (mean ± SD, n = 5). (b) Survival rate of C6 tumor-bearing mice after various treatments (mean ± SD, n = 5).

G5.NHAc-FI-HPAO-(PEG-MAL)-(*m*PEG) dendrimers (0.4 μM, 4 μM) under similar conditions. This is due to the specific cellular internalization of the CTX-targeted multifunctional dendrimers into the cytoplasm of the cells. These results indicate that only CTX-modified dendrimers can be specifically uptaken by C6 cells. On the basis of the confirmation of flow cytometric assay and confocal microscopic imaging, we can conclude that the formed G5.NHAc-FI-HPAO-(PEG-CTX)-(*m*PEG) dendrimers are able to specifically target cancer cells overexpressing MMP2 via receptor-mediated binding and endocytosis.

Targeted Tumor SPECT Imaging *in Vivo*. The feasibility to use the ^{131}I-G5.NHAc-HPAO-(PEG-CTX)-(*m*PEG) dendrimers for targeted tumor SPECT imaging was next explored (Figure 5). No visible tumor SPECT signal was observed for the mice treated with either the ^{131}I-G5.NHAc-HPAO-(PEG-CTX)-(*m*PEG) dendrimers or the ^{131}I-G5.NHAc-HPAO-(PEG-MAL)-(*m*PEG) dendrimers at 5 min, 30 min, 1 h, 2 h, and 4 h postinjection (Figure 5a). At 6, 15, and 24 h postinjection, the tumors of mice treated with the CTX-targeted dendrimer display much high SPECT signal intensity than those treated with the nontargeted dendrimer (Figure 5b). At 24 h postinjection, the tumor SPECT signal descends for both targeted and nontargeted groups, indicating that the dendrimer nanodevice can be metabolized and thus result in different biodistribution behaviors with the time postinjection. However, the SPECT signal intensity of tumors treated with the CTX-targeted dendrimer is still much higher than that treated with the nontargeted dendrimer at 24 h postinjection (p < 0.001). This highlights the role played by CTX-mediated targeting, rendering the dendrimers with enhanced accumulation in the tumor area.

To further confirm the significant difference in SPECT signal intensity of tumors treated with ^{131}I-G5.NHAc-HPAO-(PEG-CTX)-(*m*PEG) or ^{131}I-G5.NHAc-HPAO-(PEG-MAL)-(*m*PEG) dendrimers, *ex vivo* tumors were scanned at 15 h postinjection (Figure 5c). Clearly, the tumors treated with the ^{131}I-G5.NHAc-HPAO-(PEG-CTX)-(*m*PEG) dendrimer display much higher SPECT signal intensity than those treated with

DOI: 10.1021/acsami.5b05836
ACS Appl. Mater. Interfaces 2015, 7, 19798−19808

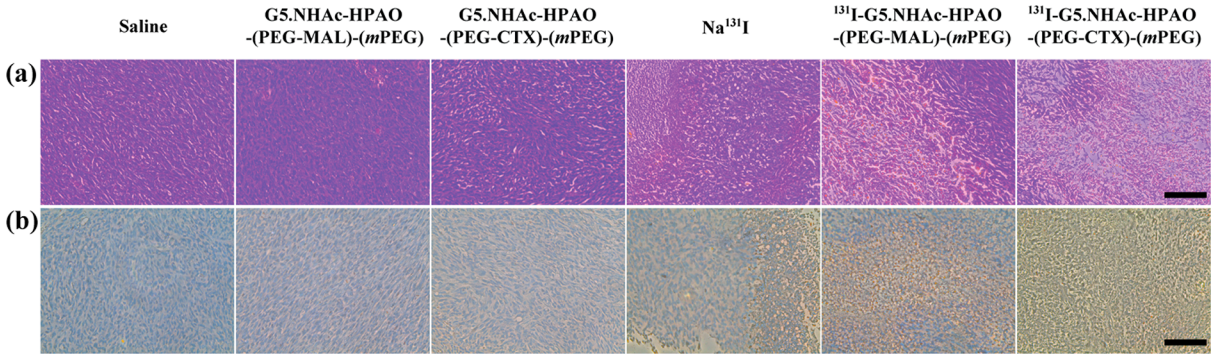

Figure 7. Representative H&E staining (a) and TUNEL assay (b) of C6 xenografted tumors treated with saline, G5.NHAc-HPAO-(PEG-MAL)-(*m*PEG), G5.NHAc-HPAO-(PEG-CTX)-(*m*PEG), $Na^{131}I$, ^{131}I-G5.NHAc-HPAO-(PEG-MAL)-(*m*PEG), and ^{131}I-G5.NHAc-HPAO-(PEG-CTX)-(*m*PEG). The scale bar shown in both panels represents 200 μm.

the ^{131}I-G5.NHAc-HPAO-(PEG-MAL)-(*m*PEG) dendrimer at the same time point.

The biodistribution of the multifunctional dendrimers at 15 h postinjection was investigated by SPECT imaging (Figure S12, Supporting Information). The majority of the ^{131}I-G5.NHAc-HPAO-(PEG-CTX)-(*m*PEG) or ^{131}I-G5.NHAc-HPAO-(PEG-MAL)-(*m*PEG) dendrimers are accumulated in the liver, while the heart, lung, tumor, kidney, spleen, intestines, stomach, and soft tissue have a relatively low accumulation of the nanoparticles. It should be noted that there is a relatively higher tumor uptake of the ^{131}I-G5.NHAc-HPAO-(PEG-CTX)-(*m*PEG) dendrimers than the nontargeted ^{131}I-G5.NHAc-HPAO-(PEG-MAL)-(*m*PEG) dendrimers. This further confirms the specific targeting role mediated by the attached CTX moiety onto the dendrimers.

Targeted Radiotherapy of Tumors *in Vivo*. The potential to use the ^{131}I-G5.NHAc-HPAO-(PEG-CTX)-(*m*PEG) dendrimers for targeted tumor radiotherapy *in vivo* was further validated (Figure 6a). It can be seen that after treatment with the ^{131}I-G5.NHAc-HPAO-(PEG-CTX)-(*m*PEG) dendrimers, the tumor grows more slowly than the tumor mice treated with saline, $Na^{131}I$, or ^{131}I-G5.NHAc-HPAO-(PEG-MAL)-(*m*PEG) dendrimers without CTX. After treatment for 3 weeks, the tumor inhibition follows the order of ^{131}I-G5.NHAc-HPAO-(PEG-CTX)-(*m*PEG) dendrimers (7.27 $\pm$ 2.19 times) > ^{131}I-G5.NHAc-HPAO-(PEG-MAL)-(*m*PEG) dendrimers (10.67 $\pm$ 3.93 times) > $Na^{131}I$ (13.07 $\pm$ 3.20 times) > saline (16.7 $\pm$ 4.67 times). The enhanced antitumor efficacy of the ^{131}I-G5.NHAc-HPAO-(PEG-CTX)-(*m*PEG) dendrimers should be due to the CTX-mediated targeting. Furthermore, the tumor inhibition efficacy was also demonstrated by the survival rates of the tumor-bearing mice (Figure 6b). Clearly, 25% of the tumor-bearing mice treated with the ^{131}I-G5.NHAc-HPAO-(PEG-CTX)-(*m*PEG) dendrimers survive after 40 days, while all the tumor-bearing mice treated with saline are dead after 30 days. Similar percentage of living mice (25%) can be seen for the tumor mice treated with $Na^{131}I$ after 32 days and the ^{131}I-G5.NHAc-HPAO-(PEG-MAL)-(*m*PEG) dendrimers after 35 days, respectively. The lifetime of the tumor-bearing mice can be greatly prolonged after treated with the ^{131}I-G5.NHAc-HPAO-(PEG-CTX)-(*m*PEG) dendrimers. This further demonstrates the effective radiotherapeutic efficacy of the ^{131}I-G5.NHAc-HPAO-(PEG-CTX)-(*m*PEG) dendrimers.

The tumor inhibition efficacy is solely owing to the labeled radioactive ^{131}I because there was no significant difference in tumor growth between the non-^{131}I labeled dendrimer groups (G5.NHAc-HPAO-(PEG-MAL)-(*m*PEG) and G5.NHAc-HPAO-(PEG-CTX)-(*m*PEG) dendrimers) and the saline group (Figure S13, Supporting Information). Furthermore, there was no significant difference in the weight loss of mice treated with the ^{131}I-G5.NHAc-HPAO-(PEG-MAL)-(*m*PEG), ^{131}I-G5.NHAc-HPAO-(PEG-CTX)-(*m*PEG), G5.NHAc-HPAO-(PEG-MAL)-(*m*PEG), and G5.NHAc-HPAO-(PEG-CTX)-(*m*PEG) dendrimers (Figure S14, Supporting Information). This suggests that the multifunctional dendrimers before and after ^{131}I labeling do not cause any apparent *in vivo* toxicity.

H&E and TUNEL staining were further used to assess the therapeutic effect of the developed ^{131}I-labeled multifunctional dendrimers in vivo (Figure 7). As shown in H&E staining (Figure 7a), necrotic regions were only observed in the mice treated with materials containing radioactive ^{131}I and the necrotic area follows the order of ^{131}I-G5.NHAc-HPAO-(PEG-CTX)-(*m*PEG) dendrimers > ^{131}I-G5.NHAc-HPAO-(PEG-MAL)-(*m*PEG) dendrimers > free $Na^{131}I$. In contrast, tumor cells had no necrosis after treated with saline, G5.NHAc-HPAO-(PEG-MAL)-(*m*PEG) dendrimers, and G5.NHAc-HPAO-(PEG-CTX)-(*m*PEG) dendrimers.

Meanwhile, the tumor inhibition efficacy of the ^{131}I-G5.NHAc-HPAO-(PEG-CTX)-(*m*PEG) dendrimers was also tested by TUNEL assay (Figure 7b). Apparently, the positive staining of apoptotic cells were solely observed in the tumor sections treated with the ^{131}I-related materials, and the region of apoptotic cells follows the sequence of ^{131}I-G5.NHAc-HPAO-(PEG-CTX)-(*m*PEG) dendrimers > ^{131}I-G5.NHAc-HPAO-(PEG-MAL)-(*m*PEG) dendrimers > free $Na^{131}I$. The tumors treated with saline, G5.NHAc-HPAO-(PEG-MAL)-(*m*PEG), and G5.NHAc-HPAO-(PEG-CTX)-(*m*PEG) dendrimers show extremely few positive apoptotic cells in the tumor sections. This was further confirmed by quantitative analysis of cell apoptosis rate (Figure S15, Supporting Information). The cell apoptosis rates of tumors treated with the ^{131}I-G5.NHAc-HPAO-(PEG-CTX)-(*m*PEG) dendrimers, ^{131}I-G5.NHAc-HPAO-(PEG-MAL)-(*m*PEG) dendrimers, and $Na^{131}I$ were 76.6%, 42.8%, and 24.1%, respectively, while those of tumors treated with the materials not related to ^{131}I do not display apparent cell apoptosis, approximately similar to the saline control. The H&E and TUNEL staining results indicate that the CTX modification renders the ^{131}I-G5.NHAc-HPAO-(PEG-CTX)-(*m*PEG) dendrimers with targeting specificity to the MMP2-overexpressing tumors for effective radiotherapy.

Finally, we investigated the potential toxicity of the multifunctional dendrimers before and after ^{131}I-labeling via

DOI: 10.1021/acsami.5b05836
ACS Appl. Mater. Interfaces 2015, 7, 19798−19808

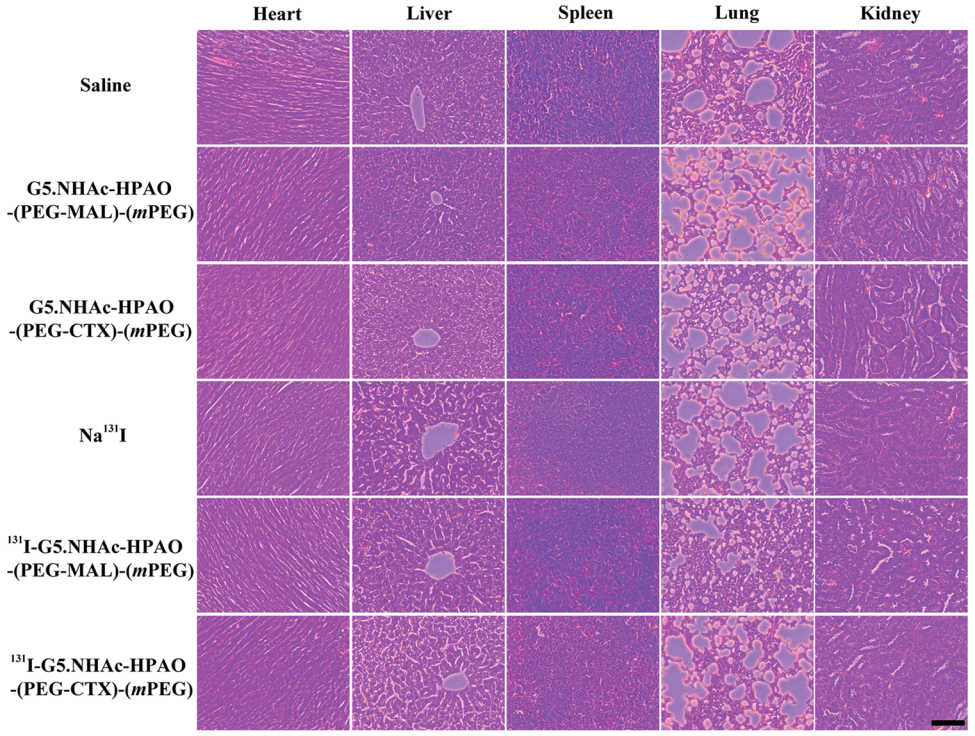

Figure 8. H&E-stained tissue sections of major organs including heart, liver, spleen, lung, and kidney from survived mice treated with saline, G5.NHAc-HPAO-(PEG-MAL)-(*m*PEG), G5.NHAc-HPAO-(PEG-CTX)-(*m*PEG), $Na^{131}I$, ^{131}I-G5.NHAc-HPAO-(PEG-MAL)-(*m*PEG), and ^{131}I-G5.NHAc-HPAO-(PEG-CTX)-(*m*PEG), respectively. The scale bar (applied for all panels) represents 200 μm.

H&E staining of the major organs including the heart, liver, spleen, lung, and kidney (Figure 8). Apparently, no obvious organ damage or abnormalities can be seen. This suggests that the multifunctional dendrimers before and after ^{131}I-labeling have good organ compatibility.

CONCLUSION

In summary, we developed an ^{131}I-labeled multifunctional dendrimer nanodevice for targeted tumor SPECT imaging and radiotherapy. *Via* the versatile dendrimer nanotechnology and PEGylation conjugation chemistry, targeting ligand CTX and HPAO can be linked onto the dendrimer platform. Through the HPAO phenol group, ^{131}I can be effectively labeled onto the dendrimer surface with a relatively high radiochemical purity and stability. With the linked CTX, the multifunctional dendrimers are able to be used as a nanoprobe for targeted SPECT imaging and radiotherapy of MMP2-overexpressing xenografted glioma model *in vivo*. The formed ^{131}I-labeled multifunctional dendrimers with good cytocompatibility and organ compatibility may be used as a promising nanoplatform for SPECT imaging and radiotherapy of different types of MMP2-overexpressing cancer.

ASSOCIATED CONTENT

Supporting Information

The Supporting Information is available free of charge on the ACS Publications website at DOI: 10.1021/acsami.5b05836.

Additional molecular structure information on the dendrimers and experimental data related to the zeta-potential, hydrodynamic size, radiochemical evaluation of the materials, NMR spectra of the dendrimeric materials, and *in vitro* and *in vivo* evaluation of the materials (PDF)

AUTHOR INFORMATION

Corresponding Authors

*E-mail: zhaojinhua1963@126.com.
*E-mail: xshi@dhu.edu.cn.

Author Contributions

⊥L. Zhao and J. Zhu contributed equally to this work.

Notes

The authors declare no competing financial interest.

ACKNOWLEDGMENTS

This research is financially supported by the National Natural Science Foundation of China (Grants 21273032 and 81171368), the Ph.D. Programs Foundation of Ministry of Education of China (Grant 20130075110004), the Funds for the International Cooperation and Exchange of the National Natural Science Foundation of China (Grant 81381340177), the Program for Professor of Special Appointment (Eastern Scholar) at Shanghai Institutions of Higher Learning, and the Shanghai Municipal Commission of Health and Family Planning (Grant 20134y160). J.Z. thanks the support from the Chinese Universities Scientific Fund (Grant BCZD201503).

REFERENCES

(1) Jemal, A.; Bray, F.; Center, M. M.; Ferlay, J.; Ward, E.; Forman, D. Global Cancer Statistics. *Ca-Cancer J. Clin.* **2011**, *61*, 69−90.
(2) Siegel, R.; Ma, J.; Zou, Z.; Jemal, A. Cancer Statistics, 2014. *Ca-Cancer J. Clin.* **2014**, *64*, 9−29.
(3) Siegel, R.; Naishadham, D.; Jemal, A. Cancer Statistics, 2012. *Ca-Cancer J. Clin.* **2012**, *62*, 10−29.
(4) Siegel, R.; Naishadham, D.; Jemal, A. Cancer Statistics, 2013. *Ca-Cancer J. Clin.* **2013**, *63*, 11−30.

DOI: 10.1021/acsami.5b05836
ACS Appl. Mater. Interfaces 2015, 7, 19798−19808

(5) DeSantis, C. E.; Lin, C. C.; Mariotto, A. B.; Siegel, R. L.; Stein, K. D.; Kramer, J. L.; Alteri, R.; Robbins, A. S.; Jemal, A. Cancer Treatment and Survivorship Statistics, 2014. *Ca-Cancer J. Clin.* **2014**, *64*, 252−271.
(6) Peer, D.; Karp, J. M.; Hong, S.; FaroKhzad, O. C.; Margalit, R.; Langer, R. Nanocarriers as an Emerging Platform for Cancer Therapy. *Nat. Nanotechnol.* **2007**, *2*, 751−760.
(7) Ferrari, M. Cancer Nanotechnology: Opportunities and Challenges. *Nat. Rev. Cancer* **2005**, *5*, 161−171.
(8) Davis, M. E.; Chen, Z.; Shin, D. M. Nanoparticle Therapeutics: An Emerging Treatment Modality for Cancer. *Nat. Rev. Drug Discovery* **2008**, *7*, 771−782.
(9) Wang, X.; Yang, L.; Chen, Z.; Shin, D. M. Application of Nanotechnology in Cancer Therapy and Imaging. *Ca-Cancer J. Clin.* **2008**, *58*, 97−110.
(10) Michalet, X.; Pinaud, F. F.; Bentolila, L. A.; Tsay, J. M.; Doose, S.; Li, J. J.; Sundaresan, G.; Wu, A. M.; Gambhir, S. S.; Weiss, S. Quantum Dots for Live Cells, in Vivo Imaging, and Diagnostics. *Science* **2005**, *307*, 538−544.
(11) Kim, Y.; Kim, S. H.; Tanyeri, M.; Katzenellenbogen, J. A.; Schroeder, C. M. Dendrimer Probes for Enhanced Photostability and Localization in Fluorescence Imaging. *Biophys. J.* **2013**, *104*, 1566−1575.
(12) Yang, H.; Zhuang, Y.; Hu, H.; Du, X.; Zhang, C.; Shi, X.; Wu, H.; Yang, S. Silica-Coated Manganese Oxide Nanoparticles as a Platform for Targeted Magnetic Resonance and Fluorescence Imaging of Cancer Cells. *Adv. Funct. Mater.* **2010**, *20*, 1733−1741.
(13) Lim, E.-K.; Kang, B.; Choi, Y.; Jang, E.; Han, S.; Lee, K.; Suh, J.-S.; Haam, S.; Huh, Y.-M. Gadolinium-Based Nanoparticles for Highly Efficient T_1-Weighted Magnetic Resonance Imaging. *Nanotechnology* **2014**, *25*, 245103−245110.
(14) Boote, E.; Fent, G.; Kattumuri, V.; Casteel, S.; Katti, K.; Chanda, N.; Kannan, R.; Katti, K.; Churchill, R. Gold Nanoparticle Contrast in a Phantom and Juvenile Swine: Models for Molecular Imaging of Human Organs Using X-Ray Computed Tomography. *Acad. Radiol.* **2010**, *17*, 410−417.
(15) Wang, H.; Zheng, L.; Peng, C.; Guo, R.; Shen, M.; Shi, X.; Zhang, G. Computed Tomography Imaging of Cancer Cells Using Acetylated Dendrimer-Entrapped Gold Nanoparticles. *Biomaterials* **2011**, *32*, 2979−2988.
(16) Jin, S.-E.; Jin, H.-E.; Hong, S.-S. Targeted Delivery System of Nanobiomaterials in Anticancer Therapy: From Cells to Clinics. *BioMed Res. Int.* **2014**, *2014*, 814208.
(17) Kraft, J. C.; Freeling, J. P.; Wang, Z.; Ho, R. J. Y. Emerging Research and Clinical Development Trends of Liposome and Lipid Nanoparticle Drug Delivery Systems. *J. Pharm. Sci.* **2014**, *103*, 29−52.
(18) Dobson, J. Gene Therapy Progress and Prospects: Magnetic Nanoparticle-Based Gene Delivery. *Gene Ther.* **2006**, *13*, 283−287.
(19) Perry, J. L.; Herlihy, K. P.; Napier, M. E.; Desimone, J. M. PRINT: A Novel Platform toward Shape and Size Specific Nanoparticle Theranostics. *Acc. Chem. Res.* **2011**, *44*, 990−998.
(20) Xie, J.; Jon, S. Magnetic Nanoparticle-Based Theranostics. *Theranostics* **2012**, *2*, 122−124.
(21) Xing, Y.; Zhao, J.; Conti, P. S.; Chen, K. Radiolabeled Nanoparticles for Multimodality Tumor Imaging. *Theranostics* **2014**, *4*, 290−306.
(22) Beyer, T.; Townsend, D. W.; Brun, T.; Kinahan, P. E.; Charron, M.; Roddy, R.; Jerin, J.; Young, J.; Byars, L.; Nutt, R. A Combined PET/CT Scanner for Clinical Oncology. *J. Nucl. Med.* **2000**, *41*, 1369−1379.
(23) Bar-Shalom, R.; Yefremov, N.; Guralnik, L.; Gaitini, D.; Frenkel, A.; Kuten, A.; Altman, H.; Keidar, Z.; Israel, O. Clinical Performance of PET/CT in Evaluation of Cancer: Additional Value for Diagnostic Imaging and Patient Management. *J. Nucl. Med.* **2003**, *44*, 1200−1209.
(24) Schoder, H.; Larson, S. M.; Yeung, H. W. D. PET/CT in Oncology: Integration into Clinical Management of Lymphoma, Melanoma, and Gastrointestinal Malignancies. *J. Nucl. Med.* **2004**, *45*, 72S−81S.
(25) Garibotto, V.; Heinzer, S.; Vulliemoz, S.; Guignard, R.; Wissmeyer, M.; Seeck, M.; Lovblad, K.-O.; Zaidi, H.; Ratib, O.; Vargas, M.-I. Clinical Applications of Hybrid PET/MRI in Neuroimaging. *Clin. Nucl. Med.* **2013**, *38*, E13−E18.
(26) Avram, A. M. Radioiodine Scintigraphy with SPECT/CT: An Important Diagnostic Tool for Thyroid Cancer Staging and Risk Stratification. *J. Nucl. Med.* **2012**, *53*, 754−764.
(27) Tatsumi, M.; Cohade, C.; Mourtzikos, K.; Fishman, E. K.; Wahl, R. L. Initial Experience with FDG-PET/CT in the Evaluation of Breast Cancer. *Eur. J. Nucl. Med. Mol. Imaging* **2006**, *33*, 254−262.
(28) Bailey, D. L.; Willowson, K. P. Quantitative SPECT/CT: SPECT Joins PET as a Quantitative Imaging Modality. *Eur. J. Nucl. Med. Mol. Imaging* **2014**, *41*, S17−S25.
(29) Mariani, G.; Bruselli, L.; Kuwert, T.; Kim, E. E.; Flotats, A.; Israel, O.; Dondi, M.; Watanabe, N. A Review on the Clinical Uses of SPECT/CT. *Eur. J. Nucl. Med. Mol. Imaging* **2010**, *37*, 1959−1985.
(30) Grassi, I.; Nanni, C.; Allegri, V.; Morigi, J. J.; Montini, G. C.; Castellucci, P.; Fanti, S. The Clinical Use of PET with (11)C-Acetate. *Am. J. Nucl. Med. Mol. Imaging* **2012**, *2*, 33−47.
(31) Das, T.; Pillai, M. R. A. Options to Meet the Future Global Demand of Radionuclides for Radionuclide Therapy. *Nucl. Med. Biol.* **2013**, *40*, 23−32.
(32) Dash, A.; Knapp, F. F. R.; Pillai, M. R. A. Targeted Radionuclide Therapy-An Overview. *Curr. Radiopharm.* **2013**, *6*, 152−180.
(33) Kassis, A. I.; Adelstein, S. J. Radiobiologic Principles in Radionuclide Therapy. *J. Nucl. Med.* **2005**, *46*, 4S−12S.
(34) D'Huyvetter, M.; Xavier, C.; Caveliers, V.; Lahoutte, T.; Muyldermans, S.; Devoogdt, N. Radiolabeled Nanobodies as Theranostic Tools in Targeted Radionuclide Therapy of Cancer. *Expert Opin. Drug Delivery* **2014**, *11*, 1939−1954.
(35) Chen, L.; Luo, Q.; Shen, Y.; Yu, Y.; Yuan, Z.; Lu, H.; Zhu, R. Incremental Value of (131)I SPECT/CT in the Management of Patients with Differentiated Thyroid Carcinoma. *J. Nucl. Med.* **2008**, *49*, 1952−1957.
(36) Buckley, S. E.; Chittenden, S. J.; Saran, F. H.; Meller, S. T.; Flux, G. D. Whole-Body Dosimetry for Individualized Treatment Planning of I-131-MIBG Radionuclide Therapy for Neuroblastoma. *J. Nucl. Med.* **2009**, *50*, 1518−1524.
(37) Shi, S.; Zhang, M.; Guo, R.; Miao, Y.; Hu, J.; Xi, Y.; Li, B. In Vivo Molecular Imaging and Radionuclide (I-131) Therapy of Human Nasopharyngeal Carcinoma Cells Transfected with a Lentivirus Expressing Sodium Iodide Symporter. *PLoS One* **2015**, *10*, e0116531.
(38) Liu, H.; Wang, H.; Xu, Y.; Guo, R.; Wen, S.; Huang, Y.; Liu, W.; Shen, M.; Zhao, J.; Zhang, G.; Shi, X. Lactobionic Acid-Modified Dendrimer-Entrapped Gold Nanoparticles for Targeted Computed Tomography Imaging of Human Hepatocellular Carcinoma. *ACS Appl. Mater. Interfaces* **2014**, *6*, 6944−6953.
(39) Jin, L.; Zeng, X.; Liu, M.; Deng, Y.; He, N. Current Progress in Gene Delivery Technology Based on Chemical Methods and Nano-Carriers. *Theranostics* **2014**, *4*, 240−255.
(40) Lee, J.-M.; Yoon, T.-J.; Cho, Y.-S. Recent Developments in Nanoparticle-Based siRNA Delivery for Cancer Therapy. *BioMed Res. Int.* **2013**, *2013*, 782041.
(41) Masserini, M. Nanoparticles for Brain Drug Delivery. *ISRN Biochem.* **2013**, *2013*, 238428.
(42) Li, N.; Li, N.; Yi, Q.; Luo, K.; Guo, C.; Pan, D.; Gu, Z. Amphiphilic Peptide Dendritic Copolymer-Doxorubicin Nanoscale Conjugate Self-Assembled to Enzyme-Responsive Anti-Cancer Agent. *Biomaterials* **2014**, *35*, 9529−9545.
(43) She, W.; Pan, D.; Luo, K.; He, B.; Cheng, G.; Zhang, C.; Gu, Z. PEGylated Dendrimer-Doxorubicin Cojugates as pH-Sensitive Drug Delivery Systems: Synthesis and in Vitro Characterization. *J. Biomed. Nanotechnol.* **2015**, *11*, 964−978.
(44) Zhang, R.; Luo, K.; Yang, J.; Sima, M.; Sun, Y.; Janát-Amsbury, M. M.; Kopeček, J. Synthesis and Evaluation of a Backbone Biodegradable Multiblock HPMA Copolymer Nanocarrier for the Systemic Delivery of Paclitaxel. *J. Controlled Release* **2013**, *166*, 66−74.
(45) Pan, D.; she, W.; Guo, C.; Luo, K.; Yi, Q.; Gu, Z. PEGylated Dendritic Diaminocyclohexyl-Platinum (II) Conjugates as pH-

DOI: 10.1021/acsami.5b05836
ACS Appl. Mater. Interfaces 2015, 7, 19798−19808

Responsive Drug Delivery Vehicles with Enhanced Tumor Accumulation and Antitumor Efficacy. *Biomaterials* **2014**, *35*, 10080−10092.
(46) Fu, F. F.; Wu, Y. L.; Zhu, J. Y.; Wen, S. H.; Shen, M. W.; Shi, X. Y. Multifunctional Lactobionic Acid-Modified Dendrimers for Targeted Drug Delivery to Liver Cancer Cells: Investigating the Role Played by PEG Spacer. *ACS Appl. Mater. Interfaces* **2014**, *6*, 16416−16425.
(47) Majoros, I. J.; Thomas, T. P.; Mehta, C. B.; Baker, J. R. Poly(amidoamine) Dendrimer-Based Multifunctional Engineered Nanodevice for Cancer Therapy. *J. Med. Chem.* **2005**, *48*, 5892−5899.
(48) Mullen, D. G.; Fang, M.; Desai, A.; Baker, J. R., Jr.; Orr, B. G.; Holl, M. M. B. A Quantitative Assessment of Nanoparticle-Ligand Distributions: Implications for Targeted Drug and Imaging Delivery in Dendrimer Conjugates. *ACS Nano* **2010**, *4*, 657−670.
(49) Shi, X.; Wang, S.; Meshinchi, S.; Van Antwerp, M. E.; Bi, X.; Lee, I.; Baker, J. R., Jr. Dendrimer-Entrapped Gold Nanoparticles as a Platform for Cancer-Cell Targeting and Imaging. *Small* **2007**, *3*, 1245−1252.
(50) Menjoge, A. R.; Kannan, R. M.; Tomalia, D. A. Dendrimer-Based Drug and Imaging Conjugates: Design Considerations for Nanomedical Applications. *Drug Discovery Today* **2010**, *15*, 171−185.
(51) Wang, S. H.; Shi, X.; Van Antwerp, M.; Cao, Z.; Swanson, S. D.; Bi, X.; Baker, J. R., Jr. Dendrimer-Functionalized Iron Oxide Nanoparticles for Specific Targeting and Imaging of Cancer Cells. *Adv. Funct. Mater.* **2007**, *17*, 3043−3050.
(52) Steichen, S. D.; Caldorera-Moore, M.; Peppas, N. A. A Review of Current Nanoparticle and Targeting Moieties for the Delivery of Cancer Therapeutics. *Eur. J. Pharm. Sci.* **2013**, *48*, 416−427.
(53) Wang, Y.; Guo, R.; Cao, X.; Shen, M.; Shi, X. Encapsulation of 2-Methoxyestradiol within Multifunctional Poly(amidoamine) Dendrimers for Targeted Cancer Therapy. *Biomaterials* **2011**, *32*, 3322−3329.
(54) Criscione, J. M.; Dobrucki, L. W.; Zhuang, Z. W.; Papademetris, X.; Simons, M.; Sinusas, A. J.; Fahmy, T. M. Development and Application of a Multimodal Contrast Agent for SPECT/CT Hybrid Imaging. *Bioconjugate Chem.* **2011**, *22*, 1784−1792.
(55) Zhang, Y.; Sun, Y.; Xu, X.; Zhu, H.; Huang, L.; Zhang, X.; Qi, Y.; Shen, Y.-M. Radiosynthesis and Micro-SPECT Imaging of Tc-99m-Dendrimer Poly(amido)-Amine Folic Acid Conjugate. *Bioorg. Med. Chem. Lett.* **2010**, *20*, 927−931.
(56) Zhang, Y.; Sun, Y.; Xu, X.; Zhang, X.; Zhu, H.; Huang, L.; Qi, Y.; Shen, Y.-M. Synthesis, Biodistribution, and Microsingle Photon Emission Computed Tomography (SPECT) Imaging Study of Technetium-99m Labeled PEGylated Dendrimer Poly(amidoamine) (PAMAM)-Folic Acid Conjugates. *J. Med. Chem.* **2010**, *53*, 3262−3272.
(57) Graf, N.; Mokhtari, T. E.; Papayannopoulos, I. A.; Lippard, S. J. Platinum(IV)-Chlorotoxin (CTX) Conjugates for Targeting Cancer Cells. *J. Inorg. Biochem.* **2012**, *110*, 58−63.
(58) Sun, C.; Veiseh, O.; Gunn, J.; Fang, C.; Hansen, S.; Lee, D.; Sze, R.; Ellenbogen, R. G.; Olson, J.; Zhang, M. In Vivo MRI Detection of Gliomas by Chlorotoxin-Conjugated Superparamagnetic Nanoprobes. *Small* **2008**, *4*, 372−379.
(59) Park, S. I.; Kwon, B. J.; Park, J. H.; Jung, H.; Yu, K. H. Synthesis and Characterization of 3-[131I] Iodo-L-Tyrosine Grafted Fe_3O_4@ SiO_2 Nanocomposite for Single Photon Emission Computed Tomography (SPECT) and Magnetic Resonance Imaging (MRI). *J. Nanosci. Nanotechnol.* **2011**, *11*, 1818−1821.
(60) Chen, J.; Zhu, S.; Tong, L.; Li, J.; Chen, F.; Han, Y.; Zhao, M.; Xiong, W. Superparamagnetic Iron Oxide Nanoparticles Mediated I-131-hVEGF siRNA Inhibits Hepatocellular Carcinoma Tumor Growth in Nude Mice. *BMC Cancer* **2014**, *14*, 114.
(61) Zhu, J. Y.; Zheng, L. F.; Wen, S. H.; Tang, Y. Q.; Shen, M. W.; Zhang, G. X.; Shi, X. Y. Targeted Cancer Theranostics Using Alpha-Tocopheryl Succinate-Conjugated Multifunctional Dendrimer-Entrapped Gold Nanoparticles. *Biomaterials* **2014**, *35*, 7635−7646.
(62) Deshane, J.; Garner, C. C.; Sontheimer, H. Chlorotoxin Inhibits Glioma Cell Invasion via Matrix Metalloproteinase-2. *J. Biol. Chem.* **2003**, *278*, 4135−4144.
(63) Veiseh, M.; Gabikian, P.; Bahrami, S. B.; Veiseh, O.; Zhang, M.; Hackman, R. C.; Ravanpay, A. C.; Stroud, M. R.; Kusuma, Y.; Hansen, S. J.; Kwok, D.; Munoz, N. M.; Sze, R. W.; Grady, W. M.; Greenberg, N. M.; Ellenbogen, R. G.; Olson, J. M. Tumor Paint: A Chlorotoxin: Cy5.5 Bioconjugate for Intraoperative Visualization of Cancer Foci. *Cancer Res.* **2007**, *67*, 6882−6888.

DOI: 10.1021/acsami.5b05836
ACS Appl. Mater. Interfaces 2015, 7, 19798−19808